

## Sustained Augmentation in Electrical Properties of $Mn_xZn_{1-x}Fe_2O_4$ Nanoparticles Provoked by High Energy Gamma Radiation

Pranav P. Naik<sup>1\*</sup>, R. B. Tangsali<sup>1</sup>, B. Sonaye<sup>2</sup> and S. Sugur<sup>2</sup><sup>1</sup>Department of Physics, Goa University, Taleigao Plateau, Goa, 403206, India.<sup>2</sup>Goa Medical College, Goa, Bambolim, 403202, India\*Email: [drppn1987@gmail.com](mailto:drppn1987@gmail.com)

Received: 8 Aug. 2014, Revised: 4 Oct. 2014, Accepted: 9 Oct. 2014.

Published online: 1 Jan. 2015.

---

**Abstract:**

A series of the  $Mn_xZn_{1-x}Fe_2O_4$  nanoparticles with ( $x = 0.2, 0.4, 0.6$  and  $0.8$ ) were prepared by auto combustion method. Electrical transport properties of the samples were studied as a function of temperature. The pellets of powdered samples were irradiated with different doses of gamma radiation obtained from  $60Co$  source. Investigations made on irradiated samples showed substantial augmentation in the electrical properties under investigation. Both conductivity and dielectric constant were seen to rise with increasing dose of gamma radiation given to the sample. The augmentation in the properties is attributed to reorganization of cation distribution which also lowered the activation energy essential for triggering various conduction mechanisms in the samples. Increasing concentration of divalent metal ions at B site with increasing gamma radiation dose also plays a substantial proactive role in raising these properties. The observations made, were found to be highly stable with no secondary emissions.

**Keywords:** Nanoparticles, X-ray diffraction, infrared spectroscopy, cation distribution, conductivity

---

### 1. Introduction

Ferrites continue to be attractive materials for technological applications due to their coalesced properties as magnetic conductors (ferrimagnetic) and electric insulators [1]. Nanoparticles of ferrites in particular Mn-Zn ferrites are looked upon as potential candidates for newer applications in targeted drug delivery, hyperthermia, MRI agents, various bio-medical sensors, etc. Research on nanoparticle ferrites is a relatively recent advancement in this area. These materials are being revived all together as their nanoparticles show all together different properties when compared with their bulk counterparts which are being studied since last four hundred years. A good number of new methods of preparing

nano powders of these materials have evolved from the intensive study that has been going on since last few decades. Of late these materials have been partially studied for their response to high energy radiations. Gamma radiation quanta possess high energy greater than 0.1MeV. In case of Co60 the energies are multifold higher than the minimum. Co60 gives two types of wave lengths  $0.0106 \text{ \AA}$  &  $0.009 \text{ \AA}$  and the gamma ray photon possesses much higher energies than the energy required to dislocate K- shell and L-shell electrons in Mn, Zn and Fe metals. K-shell and L-shell binding energies of these metals are in the range of 0.06 MeV to 0.1MeV the highest being 0.9659 MeV for K-shell electron in Zn. Moreover gamma rays of energy higher than 1MeV are known to produce electron positron pairs near nucleus which later combine and provide recoil energy to the nucleus. So gamma rays of energy higher than 1MeV can even dislocate an atom from its site in a sample. Thus high energy gamma radiation can bring about wide ranging changes in the properties of nanoparticles and these changes can be of permanent nature [2]. However the resultant modifications would depend on total dose absorbed in the material. It is known that high dose of gamma radiation can greatly alter various properties of the materials [3]. Generation of free charges due to radiation exposure can greatly modify electrical transport properties of material and will have great impact on their application and performance [4,5]. In present article we report our interesting findings on electrical properties of gamma irradiated Mn-Zn ferrite nanoparticles.

## 2. Sample Preparation

In recent years, various methods have been developed for the synthesis of single phase ferrite nanomaterials. In present work ultrafine  $\text{Mn}_x\text{Zn}_{1-x}\text{Fe}_2\text{O}_4$  particles with  $x=0.2, 0.4, 0.6, 0.8$  were prepared using auto combustion method [6]. Acetates and nitrates were used as raw materials in stoichiometric proportions along with pre-calculated amount of Nitritotriacetic acid, as a complexing agent and Glycine as a fuel for auto combustion.

## 3. Characterization

Confirmation of cubic spinel structure was done using X-Ray Diffraction patterns of as prepared  $\text{Mn}_x\text{Zn}_{1-x}\text{Fe}_2\text{O}_4$  samples obtained on Rigaku X-Ray diffractometer ( $\lambda=1.5418\text{\AA}$ ) and infrared spectroscopy using Shimadzu FTIR 8900 Spectrometer. Electrical conductivity of the  $\text{Mn}_x\text{Zn}_{1-x}\text{Fe}_2\text{O}_4$  nanoparticles was measured over the range of 303 K to 773 K using a standard D. C. Conductivity setup. Variation of dielectric constant as a function of frequency and temperature was analyzed using Wayne Kerr precision component analyzer 6440B.

#### 4. Sample Irradiation with Gamma Rays

Nanoparticles of  $Mn_xZn_{1-x}Fe_2O_4$  ferrite samples were pressed into pallets of thickness 2mm with a diameter of 10mm under a pressure of 75 KN and exposed to different doses of gamma radiation, namely (20 Gy and 100 Gy). The gamma radiation of wavelengths  $\lambda_1 = 0.0106 \text{ \AA}$  with energy  $E_1 = 1.17 \text{ MeV}$  and  $\lambda_2 = 0.009 \text{ \AA}$  with energy  $E_2 = 1.33 \text{ MeV}$  obtained from  $^{60}Co$  source were used to irradiate nanoparticle ferrite samples for different time durations. The gamma irradiated samples were investigated for changes in structure and electrical properties. Gamma irradiated samples were investigated periodically after every two months, till six months in order to test for modifications in the properties due to aging and to test for secondary emissions.

### 5 Results And Discussion

#### 5.1 X-Ray Diffraction Analysis

Figure 1(a), represents the diffraction patterns obtained for  $Mn_xZn_{1-x}Fe_2O_4$  with  $x = 0.2, 0.4, 0.6, 0.8$  of as prepared samples. Comparison of the diffraction patterns with ICDD card 10-0319 established the fact that all samples were monophasic having a cubic spinel structure. Figure 1(b), gives the XRD pattern of as prepared  $Mn_{0.8}Zn_{0.2}Fe_2O_4$  sample and the XRD patterns of same sample irradiated with high energy gamma radiation of intensity 20 Gy and 100 Gy. The patterns show that the cubic spinel structure of the material is maintained undisturbed even after the sample is irradiated with high energy gamma radiation.

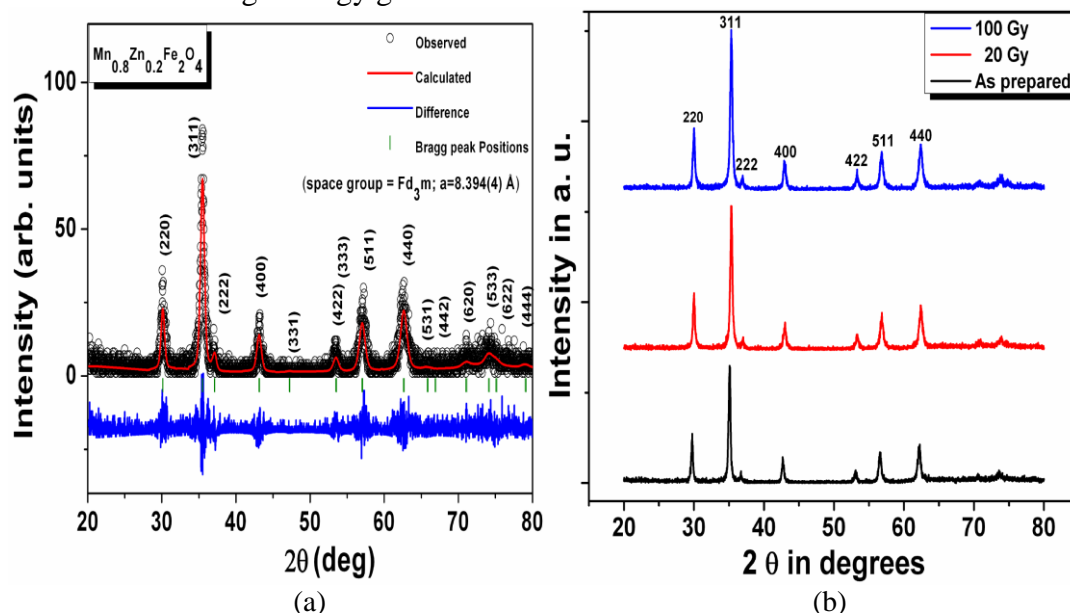


**Figure 1 (a):** Rietveld analysis of as prepared  $Mn_{0.8}Zn_{0.2}Fe_2O_4$  sample.  
**(b):** XRD pattern of as prepared nanoparticle  $Mn_{0.8}Zn_{0.2}Fe_2O_4$  and irradiated at 20 Gy and 100 Gy

Thus high energy gamma radiation has not introduced any structural disorder in the crystal structure of the sample. Observant look at the XRD patterns of irradiated sample in Figure 1(b) shows an increase in the sharpness, intensity and width of all

the peaks in the patterns. This enhancement is found to increase with increase in the radiation dose given to the sample. An increase in peak sharpness and peak intensity exhibits improved crystallinity whereas increment in the peak width is a indicator of reduction of particle size of particles in the samples. A better enhancement of these changes is observed for samples irradiated for a longer time resulting in higher dose of radiation. Similar behavior is also observed for all the samples under investigation. The particle size data of the particles in the material obtained from Scherrer's formula after applying particle strain corrections using Williamsons- Hall Plots is tabulated in Table 1.

**Table 1:** Particle size variation with gamma radiation dose absorbed

| Concentration of Mn=x | As prepared Particle Size 'D'(nm) | 20 Gy Particle Size 'D'(nm) | 100 Gy Particle Size 'D'(nm) | % Particle size change |
|-----------------------|-----------------------------------|-----------------------------|------------------------------|------------------------|
| 0.8                   | 25                                | 21                          | 20                           | 20                     |
| 0.6                   | 25                                | 17                          | 16                           | 36                     |
| 0.4                   | 27                                | 18                          | 17                           | 37                     |
| 0.2                   | 26                                | 21                          | 20                           | 23                     |

The particle size values indicated in Table 1 clearly show that there is a decrease in the particle size of the irradiated samples. This decrease in particle size can be attributed to reduction in lattice constant due to the lattice vacancies generated after irradiation causes distortion and deviation from the spinel cubic structure [7]. It may also be due to irradiation produced the compressive strain and also generated some disorder in the lattice structure (the broadening of peaks and the reduction in peak intensity) [8]. Due high energy of gamma radiation partial amorphization takes place resulting in a decrease in the average particle size [9,10].

## 5.2 Cation Distribution

The distribution of the cations at tetrahedral and octahedral sites in  $Mn_xZn_{1-x}Fe_2O_4$  mixed metal can be estimated using following equations:



Mean radius of the ion at the tetrahedral site (A- site) is given by

$$r_{tetra} = \delta r_{Zn} + \gamma r_{Mn} + (1-\gamma-\delta) r_{Fe} \quad (2)$$

And mean radius of the ion at octahedral site (B-site) is given by

$$r_{octa} = 0.5 \{ (x-\gamma) r_{Mn} + (1-x-\delta) r_{Zn} + (1+\gamma+\delta) r_{Fe} \} \quad (3)$$

On the other side the mean radius of the ions at tetrahedral site and octahedral site is given by

$$r_{tetra} = a(\sqrt{3})(u-0.25) - R_o \quad (4)$$

$$r_{octa} = a(0.625-u) - R_o \quad (5)$$

Where  $R_o$  is the radius of the oxygen ion (0.126 nm) and  $u$  is the oxygen parameter. Solving equations 2 to 5, values of  $\delta$  and  $\gamma$  can be obtained and hence cation distribution can be estimated [1,11]. Cation distribution estimates made from X-ray diffraction data of as prepared nanoparticle and irradiated nanoparticle samples are shown in Table (2, 3 and 4).

**Table 2:** Cation distribution on tetrahedral site (A-site) and octahedral site (B-site) for un-irradiated  $Mn_xZn_{1-x}Fe_2O_4$  nanoparticles.

| Concentration of Mn<br>x | $Mn_\gamma$<br>A-Site | $Zn_\delta$<br>A-Site | $Fe_{1-\delta-\gamma}$<br>A-Site | $Mn_{(x-\gamma)}$<br>B-Site | $Zn_{(1-x)-\delta}$<br>B-Site | $Fe_{(1+\delta+\gamma)}$<br>B-Site |
|--------------------------|-----------------------|-----------------------|----------------------------------|-----------------------------|-------------------------------|------------------------------------|
| 0.2                      | 0.1786                | 0.5102                | 0.3112                           | 0.0214                      | 0.2898                        | 1.6888                             |
| 0.4                      | 0.1579                | 0.4588                | 0.3833                           | 0.2421                      | 0.1412                        | 1.6167                             |
| 0.6                      | 0.3833                | 0.1302                | 0.4865                           | 0.2167                      | 0.2698                        | 1.5736                             |
| 0.8                      | 0.3869                | 0.1944                | 0.4691                           | 0.4130                      | 0.0056                        | 1.5309                             |

**Table 3:** Cation distribution on tetrahedral site (A-site) and octahedral site (B-site) for irradiated  $Mn_xZn_{1-x}Fe_2O_4$  nanoparticles irradiated with gamma radiation dose of 20Gy.

| Concentration of Mn<br>x | $Mn_\gamma$<br>A-Site | $Zn_\delta$<br>A-Site | $Fe_{1-\delta-\gamma}$<br>A-Site | $Mn_{(x-\gamma)}$<br>B-Site | $Zn_{(1-x)-\delta}$<br>B-Site | $Fe_{(1+\delta+\gamma)}$<br>B-Site |
|--------------------------|-----------------------|-----------------------|----------------------------------|-----------------------------|-------------------------------|------------------------------------|
| 0.2                      | 0.1707                | 0.4981                | 0.3312                           | 0.0293                      | 0.3019                        | 1.6688                             |
| 0.4                      | 0.1519                | 0.4485                | 0.3996                           | 0.2481                      | 0.1515                        | 1.6004                             |
| 0.6                      | 0.3598                | 0.1088                | 0.5314                           | 0.2482                      | 0.2912                        | 1.4686                             |
| 0.8                      | 0.3689                | 0.1326                | 0.4985                           | 0.4311                      | 0.0674                        | 1.5015                             |

**Table 4:** Cation distribution on tetrahedral site (A-site) and octahedral site (B-site) of irradiated  $Mn_xZn_{1-x}Fe_2O_4$  irradiated with gamma radiation dose of 100 Gy

| Concentration of Mn<br>x | $Mn_\gamma$<br>A-Site | $Zn_\delta$<br>A-Site | $Fe_{1-\delta-\gamma}$<br>A-Site | $Mn_{(x-\gamma)}$<br>B-Site | $Zn_{(1-x)-\delta}$<br>B-Site | $Fe_{(1+\delta+\gamma)}$<br>B-Site |
|--------------------------|-----------------------|-----------------------|----------------------------------|-----------------------------|-------------------------------|------------------------------------|
| 0.2                      | 0.1609                | 0.4636                | 0.3755                           | 0.0391                      | 0.3364                        | 1.6245                             |
| 0.4                      | 0.1569                | 0.4570                | 0.3861                           | 0.2431                      | 0.1430                        | 1.6139                             |
| 0.6                      | 0.3778                | 0.1267                | 0.4951                           | 0.2222                      | 0.2733                        | 1.5046                             |
| 0.8                      | 0.3580                | 0.1258                | 0.5162                           | 0.4420                      | 0.0742                        | 1.4838                             |

From cation distribution data at Table 2 and Table 4 it can be seen that for sample  $\text{Mn}_{0.2}\text{Zn}_{0.8}\text{Fe}_2\text{O}_4$  0.1707 Mn, 0.5102 Zn and 0.3112 Fe, occupancy at A site and 0.0214 Mn, 0.2898 Zn and 1.6888 Fe occupancy at B-site changes to 0.1609 Mn, 0.4636 Zn and 0.3755 Fe, occupancy at A site and 0.0391 Mn, 0.3364 Zn and 1.6245 Fe occupancy at B-site when the sample is irradiated with Gamma radiation with a dose of 100 Gy. Thus the high energy gamma radiation produces multiple exchanges between Mn, Zn and Fe at the two sites.

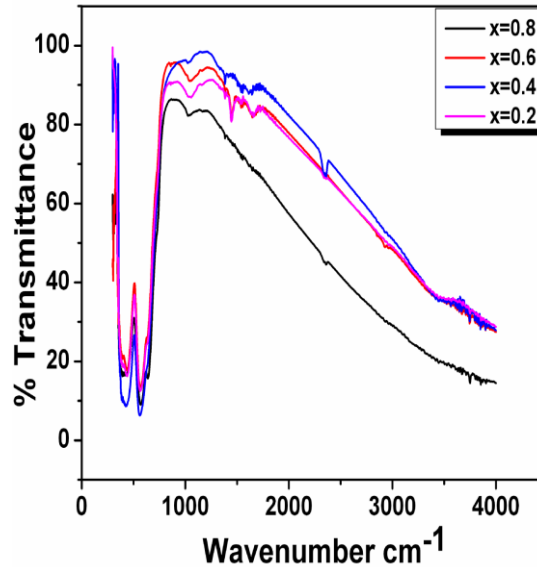


**Figure 2:** Infra Red spectra of as prepared  $\text{Mn}_x\text{Zn}_{1-x}\text{Fe}_2\text{O}_4$  nanoparticles.

### 5.3 Infrared Spectroscopy

Figure 2 shows various IR absorption peaks observed in the spectra correspond to the following vibrational modes. The  $\text{Me}_T\text{—Me}_O$  stretching vibration at  $350\text{--}330\text{ cm}^{-1}$  is of low intensity and merges with the  $\text{Me}_O\text{—O}$  stretching vibration at  $450\text{--}485\text{ cm}^{-1}$  giving a single wide band. The other broad band observed is due to  $\text{Me}_T\text{—O—Me}_O$  Stretching vibration at  $600\text{--}500\text{ cm}^{-1}$ , where O is oxygen,  $\text{Me}_O$  is metal in the octahedral site and  $\text{Me}_T$  is the metal at tetrahedral site. These are the most prominent broad stretching vibrational bands observed for ferrite samples [12].

### 5.4 Conductivity

Temperature dependence of DC conductivity ' $\sigma$ ' of as prepared and gamma irradiated nanoparticle  $\text{Mn}_x\text{Zn}_{1-x}\text{Fe}_2\text{O}_4$  samples is shown in Figure 3. Samples show typical semiconductor type behavior where in an increase in conductivity was observed with increase in temperature after initial decrease registered as a dip in almost all the conductivity curves, which is a result of phonon scattering.

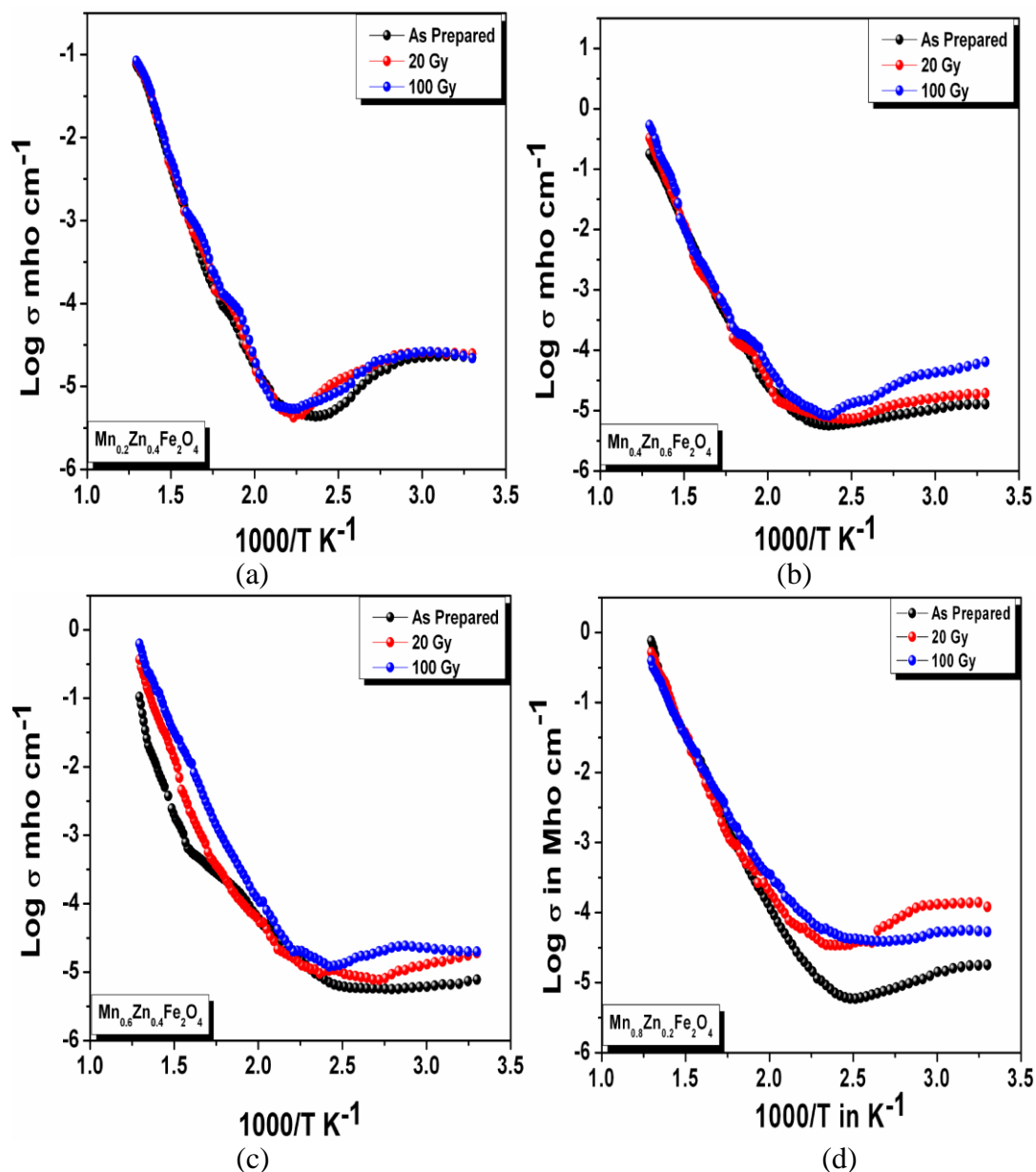


**Figure 3:** Variation of dc conductivity with  $(1000/T \text{ K}^{-1})$  for as prepared and irradiated  $\text{Mn}_x\text{Zn}_{1-x}\text{Fe}_2\text{O}_4$  ferrite nanoparticle samples.

It can be seen that the conductivity minima is sensitive to Mn concentration in the sample and towards lower temperatures with increasing Mn concentration in the samples. This is true in case of as prepared as well as gamma irradiated nanoparticle samples. However as prepared nanoparticle samples show a lower conductivity value in the lower temperature range starting from room temperature compared to the conductivity shown by gamma irradiated samples. Conduction over lower temperature range is predominantly attributed to hopping mechanism, where in conduction depends on sample temperature. However large value of conductivity in irradiated samples may be due to larger population of charge carriers in the conduction band and valance band of the material due to dislocation of K-shell and L-shell electrons by high energy gamma radiation. The higher value of conductivity for irradiated samples  $\text{Mn}_{0.4}\text{Zn}_{0.6}\text{Fe}_2\text{O}_4$  and  $\text{Mn}_{0.6}\text{Zn}_{0.4}\text{Fe}_2\text{O}_4$  clearly indicates availability of greater number of charge carriers in the conduction band presumably coming from the dislocation of K-shell and L-shell electrons from Mn and Zn metal ions in addition to Fe ions both

from A site and B site. Beyond conductivity minima, mechanisms such as  $Mn^{+2} \leftrightarrow Mn^{+3}$  and  $Zn^{+2} \leftrightarrow Zn^{+3}$  along with  $Fe^{+3} \leftrightarrow Fe^{+2}$  at B site dominate the conduction process due to thermal energy available at high temperature. It is observed that the minimum value of conductivity also increases with the increase in radiation dose which can be attributed to increase in  $Fe^{+3}/Fe^{+2}$ ,  $Mn^{+2}/Mn^{+3}$  and  $Zn^{+2}/Zn^{+3}$  concentration at octahedral site which is greatly altered due to gamma exposure [2] and is seen from cation distribution data presented in Table (2, 3 and 4). This increase is also proportionate to the Mn concentration where in maximum variation in conductivity is observed for  $x=0.8$  and minimum for  $x=0.2$ .

### 5.5 Activation energy

Activation energy has been estimated using Arrhenius equation,

$$\sigma = \sigma_0 \exp [-E_a/K_B T] \quad (6)$$

Where ( $\sigma$ ) is electrical conductivity, ( $\sigma_0$ ) is the ideal conductivity of mono-crystalline structure,  $K_B$  is Boltzmann's constant and T is temperature [13]. It is observed that activation energy essential to trigger different conduction mechanisms at different temperature ranges was greatly lowered for irradiated samples facilitating the conduction process. Activation energy values for all the nano-samples are listed below in Table (5, 6, 7 and 8).

**Table 5:** Values of Activation energy for  $Mn_{0.2}Zn_{0.8}Fe_2O_4$

| Gamma Radiation dose | Temperature Range        | Temperature Range         | Temperature Range        |
|----------------------|--------------------------|---------------------------|--------------------------|
|                      | 348K-450K                | 460K-584K                 | 634K-632K                |
| As prepared          | $3.61 \times 10^{-1} eV$ | $3.56 \times 10^{-1} eV$  | $1.45 \times 10^{-1} eV$ |
| 20 Gy                | $8.09 \times 10^{-2} eV$ | $3.43 \times 10^{-1} eV$  | $1.11 \times 10^{-1} eV$ |
| 100 Gy               | $6.55 \times 10^{-2} eV$ | $3.025 \times 10^{-1} eV$ | $1.12 \times 10^{-1} eV$ |

**Table 6:** Values of Activation energy for  $Mn_{0.4}Zn_{0.6}Fe_2O_4$

| Gamma Radiation dose | Temperature Range        | Temperature Range        | Temperature Range        |
|----------------------|--------------------------|--------------------------|--------------------------|
|                      | 303K-414K                | 434K-526K                | 558K-735K                |
| As prepared          | $7.65 \times 10^{-2} eV$ | $2.54 \times 10^{-1} eV$ | $5.63 \times 10^{-1} eV$ |
| 20 Gy                | $4.06 \times 10^{-2} eV$ | $2.35 \times 10^{-1} eV$ | $5.30 \times 10^{-1} eV$ |
| 100 Gy               | $3.21 \times 10^{-2} eV$ | $2.28 \times 10^{-1} eV$ | $5.63 \times 10^{-1} eV$ |

**Table 7:** Values of Activation energy for  $Mn_{0.6}Zn_{0.4}Fe_2O_4$

| Gamma Radiation dose | Temperature Range         | Temperature Range        | Temperature Range        |
|----------------------|---------------------------|--------------------------|--------------------------|
|                      | 303K-400K                 | 505K-632K                | 641K-740K                |
| As prepared          | $3.23 \times 10^{-2} eV$  | $4.37 \times 10^{-1} eV$ | $6.48 \times 10^{-1} eV$ |
| 20 Gy                | $1.725 \times 10^{-2} eV$ | $3.55 \times 10^{-1} eV$ | $5.79 \times 10^{-1} eV$ |
| 100 Gy               | $1.07 \times 10^{-2} eV$  | $2.11 \times 10^{-1} eV$ | $4.81 \times 10^{-1} eV$ |

**Table 8:** Values of Activation energy for  $Mn_{0.8}Zn_{0.2}Fe_2O_4$

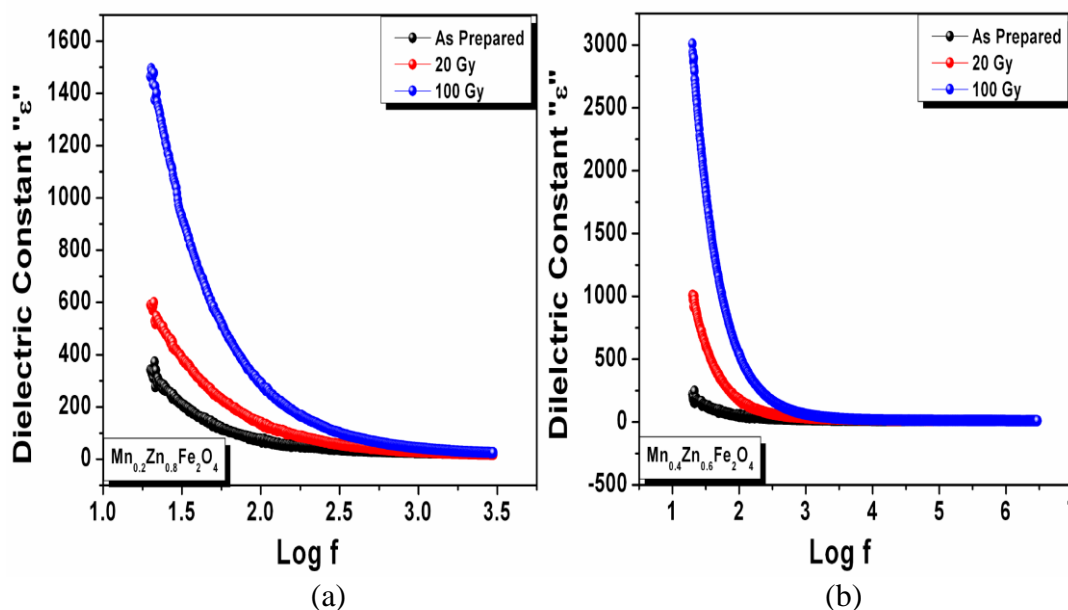
| Gamma Radiation dose | Temperature Range | Temperature Range | Temperature Range |
|----------------------|-------------------|-------------------|-------------------|
|                      | 303K-398K         | 411K-546K         | 588K-740K         |

|             |                                 |                                 |                                 |
|-------------|---------------------------------|---------------------------------|---------------------------------|
| As prepared | $5.49 \times 10^{-2} \text{eV}$ | $2.94 \times 10^{-1} \text{eV}$ | $4.73 \times 10^{-1} \text{eV}$ |
| 20 Gy       | $1.07 \times 10^{-2} \text{eV}$ | $2.08 \times 10^{-1} \text{eV}$ | $4.45 \times 10^{-1} \text{eV}$ |
| 100 Gy      | $5.17 \times 10^{-2} \text{eV}$ | $1.89 \times 10^{-1} \text{eV}$ | $4.01 \times 10^{-1} \text{eV}$ |

The activation energy has been estimated in the three different temperature zones, the low temperature zone, the mid temperature zone and the high temperature zone. It may be noted that the three temperature zones are different for the four samples. From the values listed in the Tables 5 to 8 it is evident that the activation energy in the first two zones is lower for radiated samples but in the third zone of high temperature the activation energies of radiated and as prepared nanoparticles are nearly same. This means that at high temperatures all the samples including gamma irradiated samples behave alike as all the three curves are merge with each other at these temperatures except for sample with  $x=0.6$  for sample  $\text{Mn}_{0.6}\text{Zn}_{0.4}\text{Fe}_2\text{O}_4$  the conductivity of gamma irradiated samples is higher than as prepared nanoparticle sample for a given value of temperature. Thus in irradiated samples excessive Mn in the sample  $\text{Mn}_{0.6}\text{Zn}_{0.4}\text{Fe}_2\text{O}_4$  enhances the conductivity of the sample then excessive Zn in  $\text{Mn}_{0.4}\text{Zn}_{0.6}\text{Fe}_2\text{O}_4$ .

### 5.6 Dielectric constant

In the electrical properties conductivity ‘ $\sigma$ ’, dielectric constant ‘ $\epsilon$ ’ are important parameters of ferrite as far as applications are concerned. The dielectric constant strongly depends on exchange of electrons between  $\text{Fe}^{2+}$  and  $\text{Fe}^{+3}$  ions. It has been concluded that electron exchange  $\text{Fe}^{+2}$ ,  $\text{Fe}^{+3}$  results in local displacement of charges which is responsible for polarization in ferrites. The magnitude depends upon concentration of  $\text{Fe}^{+2}$  and  $\text{Fe}^{+3}$  ion pairs present at A- site and B- site [14].



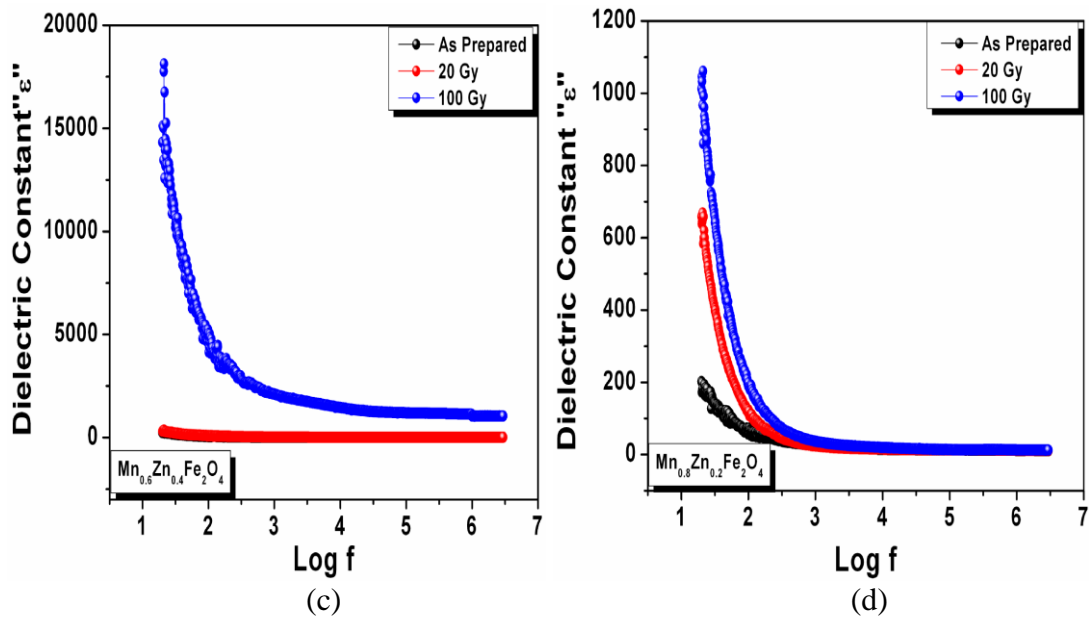


**Figure 4:** Variation of dielectric constant with frequency for as prepared and irradiated  $Mn_xZn_{1-x}Fe_2O_4$  samples

Figure 4 shows variation of dielectric constant with frequency of all as prepared and gamma irradiated  $Mn_xZn_{1-x}Fe_2O_4$  nanoparticle samples. Dielectric constant was found to decrease abruptly for the higher values of frequencies for both as prepared and irradiated nanoparticle samples which is a general trend followed by ferrites [15]. It can be seen that the dielectric constant ' $\epsilon$ ' of irradiated samples show a multifold jump from the value shown by as prepared nanoparticle sample. The dielectric constant values are sensitive to gamma radiation dose as well as Mn and Zn content in the sample. The highest value of 16383 observed for dielectric constant  $\epsilon$  at frequency 20Hz for  $Mn_{0.6}Zn_{0.4}Fe_2O_4$  nanoparticle sample irradiated with a radiation dose of sample 100Gy is seen to fall almost exponentially to a low value of 10 at high frequency of 3MHz. Whereas its unirradiated or as prepared counterpart shows a high value of 248 at 20Hz and approaches a low value of 3 at a frequency of 3MHz. Similarly all other radiated samples exhibit higher values of dielectric constants than as prepared nanoparticle samples. This fact indicates that in addition to Fe, Mn and Zn also are actively involved in the polarization of the dielectric due to dislocation of K-Shell and L-shell electrons from these atoms.

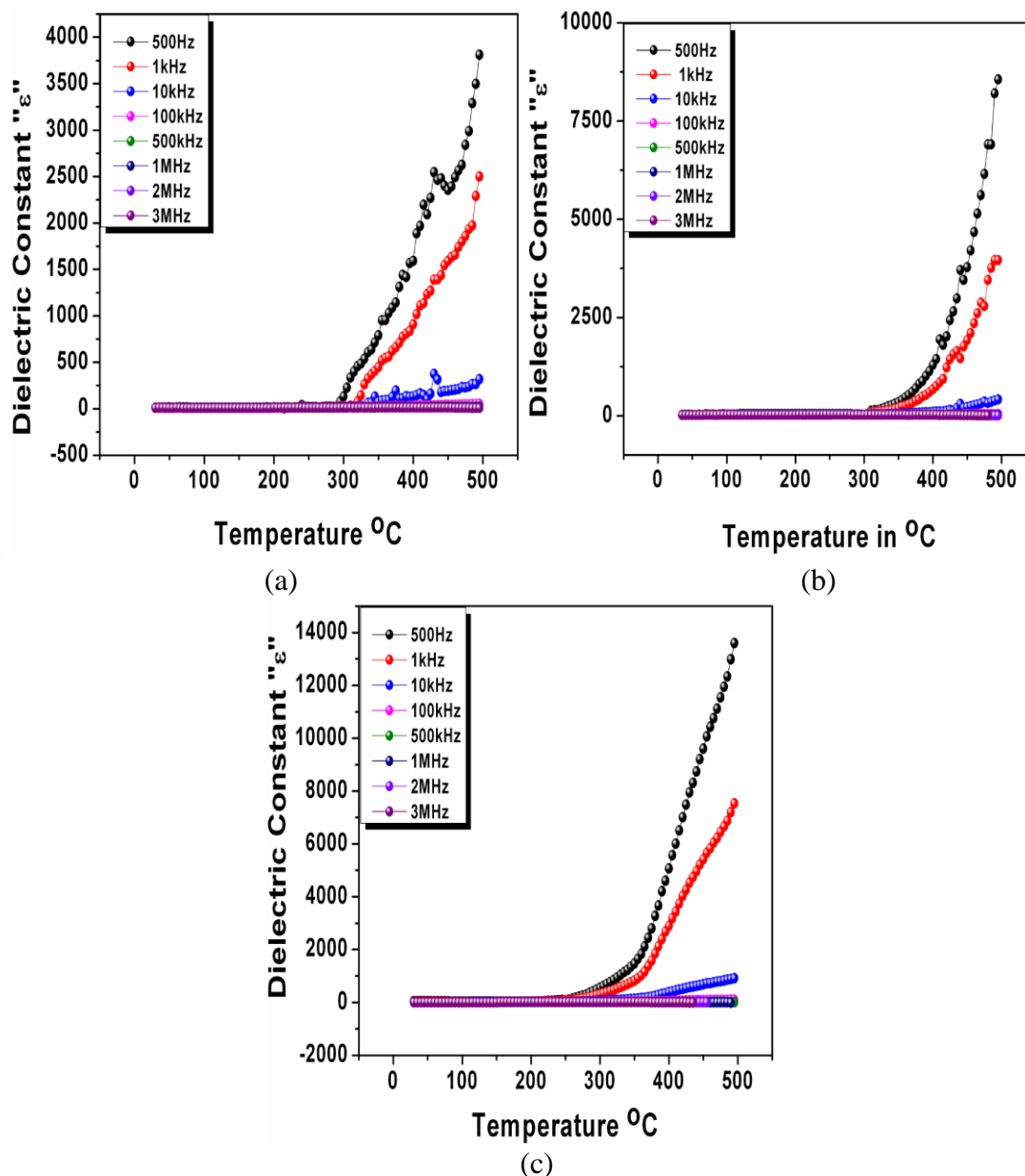


**Figure 5:** Variation of Dielectric constant with temperature for (a) as prepared  $Mn_{0.8}Zn_{0.2}Fe_2O_4$  sample, (b)  $Mn_{0.8}Zn_{0.2}Fe_2O_4$  irradiated at 20 Gy & (c)  $Mn_{0.8}Zn_{0.2}Fe_2O_4$  irradiated at 100 Gy.

All samples show increase in dielectric constant with increasing temperature. Figure 5 depicts a typical behavior of dielectric constant ‘ $\epsilon'$ ’ with temperature for both as prepared and irradiated  $Mn_{0.8}Zn_{0.2}Fe_2O_4$  nanoparticles. Increase in dielectric constant was also observed with the increase in gamma radiation dose which can be attributed to hopping rate caused from depressing the jump length with the result of more interaction between  $Mn^{3+} \leftrightarrow Mn^{2+}$  and  $Fe^{3+} \leftrightarrow Fe^{2+}$ . The field oriented electron hopping increases dielectric constant. Vacancies generated at different depths which act as trapping centers also contribute towards dielectric constant. The liberation of charge carriers from these trapping centers needs different energies. This seems to be the main reason for highest value of dielectric constant in the case of 100Gy irradiated sample [16].

## 6. Conclusion

Nanoparticle  $Mn_xZn_{1-x}Fe_2O_4$  ferrite samples with  $x=0.2, 0.4, 0.6, 0.8$  prepared by auto-combustion method were irradiated with high energy gamma radiation. Investigations carried out on electrical transport properties of these irradiated samples were compared with similar properties of as prepared nanoparticle samples. A general enhancement in the values of conductivity and dielectric constant of the irradiated samples was observed. Enhancement in electrical conductivity and dielectric constant can be accredited to increment in the conduction electrons due to dislocation of K-shell and L-shell electrons from metal ions Mn, Zn and Fe and lowering of activation energy and triggering of various hopping mechanisms at various temperatures. An alteration in the cation distribution of the gamma irradiated nanoparticles was also observed. This could be due to formation of electron positron pair formation and annihilation near the nucleus which may be responsible for providing the required dislocation energy to the atom. Repeated measurements carried out on samples over a period of six months after irradiating the samples did not show any least significant change in the properties under investigation. This establishes that the changes produced in the material are highly stable and there is no possibility of secondary emissions from the samples.

## Acknowledgment

Authors thank DST Delhi, for funding this project under Nano-initiative project received by Goa University

## References

- [1] E. Ateia, Egypt, J. Solids, Vol. (29), No. (2) (2006,)
- [2] O. M. Hemeda, M. El-Saadawy, J. Magn. Magn. Mater., 256, 2003, 63–68.
- [3] M. A. Ahmed, A. A. Ramadan, M. A. El Ahdal, M. M. Kamal, and A. Yousef, AIP Conf. Proc. 888, pp. 288-293(2007).
- [4] T. P. Ma, P. V. Dressendorfer, Wiley, New York, (1989).
- [5] Minh-Tri TA, D. Briand, B. Boudart, Y. Guhel, Microelectronic Engineering, 87, 2158 – 2162, (2010).
- [6] R. B. Tangsali, S. H. Keluskar, G. K. Naik, J. S. Budkuley, Int. J. Nanoscience, Volume: 3, Issues: 4-5, pp. 589-597(2004).
- [7] A. Tawfik, I.M. Hamada, O.M. Hemeda, J. Magn. Magn. Mater. 250, 77(2002).
- [8] A. Dogra, M. Singh, R. Kumar, Nucl. Instr. And Meth. B 207, 296- 300(2003).
- [9] B. Parvatheeswara Rao, K.H. Rao, P.S.V. Subba Rao, A. Mahesh Kumar, Y.L.N. Murthy, K. Asokan, V.V. Siva Kumar, R. Kumar, N.S. Gajbhiye, O.F. Caltun, Y.L.N. Murthy, Nucl. Instrum. Meth. B 244, 27(2006).
- [10] Asif Karim , Sagar E. Shirsath, S.J. Shukla, K.M. Jadhav, Nuclear Instruments and Methods in Physics Research B 268, 2706–2711(2010).
- [11] A. A. Yousif, M. E. Elzain, S. F. Mansour, S. A. Mazen, H. H. Sutherland, M. H. Abdalla, J. Phys. Condens. Matter., volume 6b, 5717(1994).
- [12] R. B. Tangsali, S. H. Keluskar, G. K. Naik, J. S. Budkuley , J. Mater. Sci., volume 42, 878–882(2007).
- [13] M. A. Omar, Elementary Solid State Physics, 2nd. Edition, John Wiley and Sons Inc., New York, 1975.
- [14] K. Iwachi, Jpn. J. Appl. Phys., 10, 1520 (1971).
- [15] O. S. Josyulu, J. Sobhanadri, B. Viswanatham, Rev. Roum. Chim. 26(5), 687 (1981).
- [16] N. Rezlescu, E. Rezlescu and C. Pasnicu and M. L. Craus, J. Phy. Condensed Matter 6, 5707 (1994).